Journal of Applied Electrochemistry **34**: 507–516, 2004.

Effect of heat-treatment on the mechanism and kinetics of the hydrogen evolution reaction on Ni–P + TiO_2 + Ti electrodes

B. ŁOSIEWICZ[1], A. BUDNIOK[1,*], E. RÓWIŃSKI[1], E. ŁĄGIEWKA[1] and A. LASIA[2]
[1]*Institute of Materials Science, Silesian University, 40-007 Katowice, 12 Bankowa, Poland*
[2]*Département de chimie, Université de Sherbrooke, Sherbrooke, Québec, J1K 2R1 Canada*
*(*authors for correspondence, fax: +48 32 2596929, e-mail: budniok@us.edu.pl)*

Received 11 December 2002; accepted in revised form 19 November 2003

Key words: hydrogen evolution reaction, impedance modelling, nickel based electrodes, titanium, titanium dioxide

Abstract

Composite Ni–P + TiO_2 + Ti layers were prepared by codeposition of Ni–P alloy with TiO_2 and Ti powders from a solution containing suspension of TiO_2 and Ti particles. The electrodeposition was carried out under galvanostatic conditions at room temperature. The layers exhibited an amorphous Ni–P matrix in which crystalline TiO_2 and Ti were embedded. On the deposit surface, the nonstoichiometric Ti oxide, $Ti_{10}O_{19}$, and intermetallic compounds, NiTi, formed during the electrodeposition, were also present. The heat treatment of these layers in argon leads to the crystallization of Ni–P matrix and formation of nonstoichiometric Ti oxides, detected by XRD. Electrolytic activity towards the hydrogen evolution reaction (HER) was studied on these electrode materials before and after heat treatment. The mechanism of the HER was also studied, and the kinetic parameters were determined using steady-state polarization and electrochemical impedance spectroscopy (EIS). An increase in activity occurring after heating of Ni–P + TiO_2 + Ti layers is related to TiO_2 reduction and formation of nonstoichiometric Ti oxides: $Ti_{10}O_{19}$ (400 °C), Ti_7O_{13} (500 °C) and Ti_4O_7 (800 °C). It is postulated that the increase in electrochemical activity is related to the properties of these oxides and a facility for H reduction/adsorption on their surface, as well as to the presence of NiTi intermetallics as compared with the Ni–P + TiO_2 + Ti electrode.

1. Introduction

The hydrogen evolution reaction (HER) is one of the most frequently studied electrochemical processes; nevertheless the influence of the nature of composite substrates on its kinetics is not yet well understood [1–5]. Although water electrolysis is not the cheapest method of hydrogen production it supplies hydrogen of a very high purity. Thus, new electrode materials, capable of catalytically reducing the energy barrier of the HER, are still being sought [5].

The HER is catalysed by platinum metals and to a lesser extent by iron, cobalt and nickel [1, 3, 4, 6]. Of the transition metals, only Ni is stable in concentrated alkaline solution at the hydrogen equilibrium potential [6]. To compensate for its lower catalytic activity and, simultaneously, to take advantage of its relatively low price (as compared with Pt-group metals), different methods have been applied to improve Ni electrode performance [1, 2, 7–10]. The apparent electrocatalytic activity may be increased by increasing the real surface area (e.g., Raney-type alloys) or by increasing the intrinsic (real) activity of the material by the use of alloys or composites [11–16]. The second method often involves use of electrodeposited materials.

Electrodeposited crystalline and amorphous Ni coatings, as well as Ni-based alloys and composite layers, are well known [2–10, 17–21]. Among electrodeposited composite layers materials of particular importance are deposits containing oxides (NiO, RuO_2, IrO_2, TiO_2) [2, 3, 7–9], or metals like Ti, W, Nb, Zr, which cannot be directly codeposited in metallic form from aqueous solutions [2, 3, 4, 7–10]. However, it is possible to introduce these metals in a powder form and embed them into a metal matrix. Titanium is particularly interesting because of its mechanical and electrochemical properties. In oxidizing environments Ti is covered with an oxide film and exhibits catalytic activity towards the HER [4]. As a cathode material Ti is characterized by an affinity for hydrogen and an ability to form hydrides [22, 23]. Titanium oxides are also used as activating agents in numerous electrochemical processes [2, 4, 8]. It was found that TiO_2, when inserted into the Ni–P structure, reduces the overpotential of the HER. This effect results from the catalytic action of the oxygen compounds of Ti(III) and (IV) present in the

Ni–P + TiO_2 layer [8]. It was postulated that these compounds are formed during the electrolytic deposition of the layer. Therefore, it seemed promising to prepare Ni–P + TiO_2 + Ti electrodes to combine the good physical and chemical stability of Ni–P with the high activity of TiO_2 and Ti components.

The present study was undertaken to obtain composite layers in a Ni–P system containing TiO_2 and Ti components. Our main goal was the determination of the heat treatment effect on the morphology, composition and kinetics of the HER on Ni–P + TiO_2 + Ti electrodes. The mechanism of the HER on these electrodes was studied in 5 M KOH, and the kinetic parameters were determined using steady-state polarization and EIS techniques.

2. Experimental details

2.1. *Bath composition and conditions of electrodes deposition*

To obtain composite Ni–P + TiO_2 + Ti layers the following Ni plating bath was prepared (concentrations are given in g dm^{-3}): 51 $NiSO_4 \cdot H_2O$, 10.7 NH_4Cl, 29 $NaH_2PO_2 \cdot H_2O$, 10 CH_3COONa and 8 H_3BO_3, to which 99 g dm^{-3} of TiO_2 (anatase, Loba Feinchemie, Lot. nr 17508, 100 mesh) and 10 g dm^{-3} of Ti powder (Aldrich, Lot. nr 17301, 325 mesh, 99.98%) were added and maintained in suspension by stirring at 300 rpm. The solution pH was 4.8–5.2 (CP 101 Elmetron pH-meter). Deionized water and chemicals of analytical grade (Merck, POCh Gliwice) were used for the solutions.

The electrodeposition was carried out at 25 °C, at a current density of $j = 250$ mA cm^{-2} for 25 min on a steel plate substrate (St3S, 1.0 cm^2). The substrate preparation and experimental set-up has been described previously [3]. The deposit thickness was estimated by microscopy to be about 200 μm. The layers were heated at 400, 500 and 800 °C for 10 h under a flow of argon using three deposits at each temperature.

Surface morphology was determined by a Nikon SMZ-2T stereoscopic microscope (mag. 430×). The layer surface roughness was determined using a Form Tylysurf surface analyser (Taylor Hobson). Structural investigations were conducted by XRD using a Philips diffractometer and CuK_α radiation.

Quantitative chemical analysis of the layers was determined by means of atomic absorption (AAS) using a Perkin–Elmer spectrometer. For this purpose, the layers were dissolved in HNO_3:HF solution (v/v 1:1) and the concentrations of Ni (±3%) and Ti (±2%) were determined. After dissolution of deposits, the solid undissolved TiO_2 powder was filtered, dried and weighed within accuracy of 1×10^{-5} g. Each result was an average of five samples obtained under the same conditions. The P content in the layer was determined as a difference of Ni, Ti and TiO_2 content, and the total layer mass.

Auger electron spectroscopy (AES) was used for the determination of the layer surface composition by means of a vacuum system (SP-2000 1/M) with the help of an Auger spectrometer (SEA 02). The layer surface preparation and measurements method were described elsewhere [4].

2.2. *Electrochemical measurements conditions*

All the electrochemical measurements were carried out at 25 °C in 5 M KOH solutions to which 10 g dm^{-3} of the complexing agent (sodium salt of EDTA, $C_{10}H_{14}O_8N_2Na_2 \cdot 2\ H_2O$) was added in order to avoid electrode deactivation [16]. Oxygen was removed by bubbling argon.

The HER was studied in a Pyrex® glass cell (Radiometer 1734). The counter electrode was a platinum mesh (~1 dm^2). The external Hg/HgO/5 M KOH reference electrode maintained at room temperature was connected to the cell through a bridge filled with 5 M KOH and a Luggin capillary. The experimentally determined reversible potential for the HER was time independent and was equal to −0.930 V. Data analysis and instrumentation are described elsewhere [3, 4].

The HER mechanism was determined on the basis of the dependence of both the steady-state current density j and the parameter A, the inverse of the charge-transfer resistance, determined by EIS, on the overpotential η. The rate constants of the HER were evaluated using the NLS method [1–5, 11–16].

3. Results and discussion

3.1. *Electrode composition and surface morphology*

The Ni–P + TiO_2 + Ti layer, before and after heat treatment (Figure 1(a) and (b)), showed good adhesion to the substrate and no internal stresses resulting in cracks or defoliation from the steel plate. The composite Ni–P + TiO_2 + Ti layer had a mat-grey, rough metallic surface with visible grains of embedded Ti powder and white colouration of TiO_2 on the surface (Figure 1(a)). The AAS results showed that these layers contain (wt %): 55 Ni, 16 P, 21 TiO_2 and 8 Ti. The surface of heated deposits was less developed as compared to the layer before heating. An example of the layer heated at 400 °C is shown in Figure 1(b). The heated layer surface is characterized by the presence of a different colour: red after heating at 400 °C, blue after heating at 500 °C, and green after heating at 800 °C. This phenomenon was reproducible and connected with TiO_2 reduction and formation of different nonstoichiometric Ti oxides during the heat treatment.

The cross-section showed that the thickness of the Ni–P + TiO_2 + Ti layer was about 200 and 150 μm before and after heating, respectively (Figure 1(c) and (d)). It also confirmed the composite structure of the deposit with uniformly distributed Ti and TiO_2 grains, and more

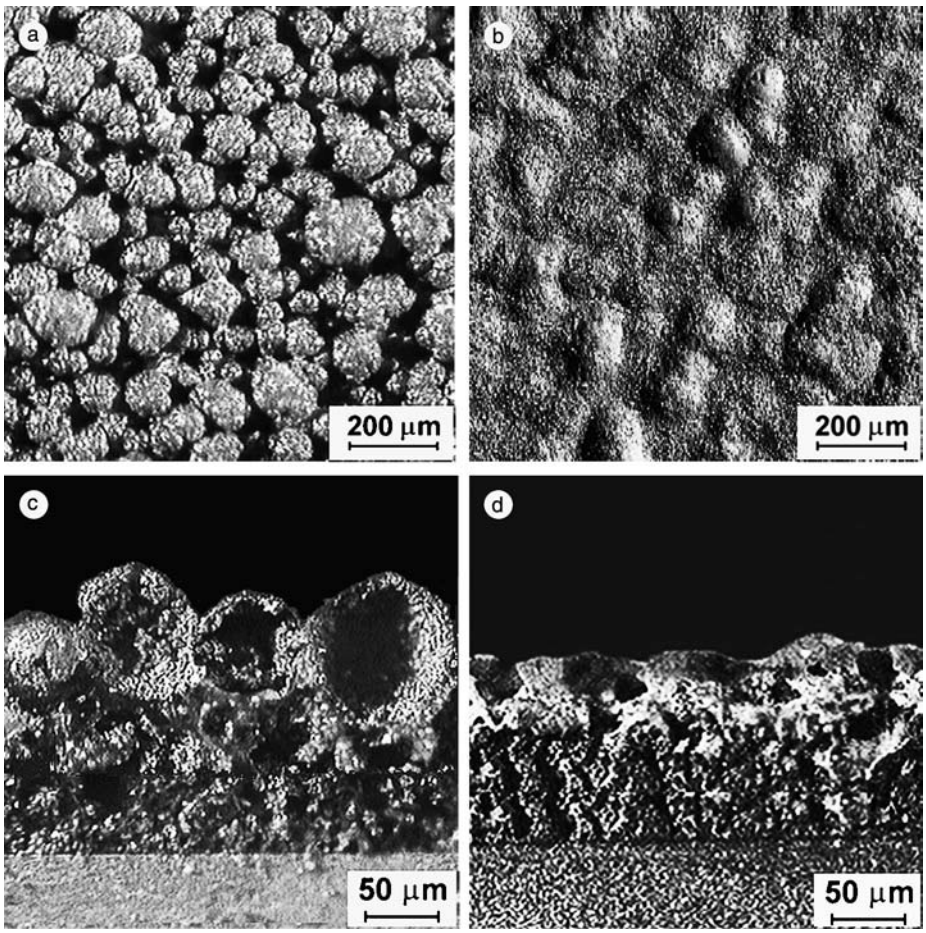

Fig. 1. Surface morphology of the Ni–P + TiO_2 + Ti layer before (a) and after heating at 400 °C (b), and the appropriate microscopic cross-sections (c, d).

developed surface of the as-deposited layer in comparison with that of the heated deposit surface.

The roughness factor, defined as an average distance of adjacent (local) vertexes, *RS*, was experimentally determined. The surface roughness profiles for investigated layers are displayed in Figure 2(a) and (b). The Ni–P + TiO_2 + Ti layer surface was characterized by the value of $RS = 109.9$ μm (Figure 2(a)) which was over two times larger than $RS = 54.1$ μm (Figure 2(b)) determined for the heated layer. This indicates that the heat treatment of those layers caused the Ni–P matrix crystallization and the interaction between the composite components resulting in a more compact structure and a decreased layer surface development.

3.2. *AES measurements*

Figure 3 shows Auger spectra of the surface of the Ni–P + TiO_2 + Ti layer. The line identification was carried out on the basis of the spectrogram standard contained in the catalogue [25] and [26, 27]. The registered Auger Ti (LMV) curve was smoothed [27]. The Auger line intensity measured by the peak-to-peak method was analysed, and the chemical analysis based on element identification using the Auger peak parameters like the energy position (E) and the line intensity, was applied. Table 1 contains the results of this analysis of the energy position of the analysed element Auger lines.

From the Auger Ti (LMV) position (Figure 3) it follows that Ti on the Ni–P + TiO_2 + Ti layer surface appears in three forms: (a) as TiO_2 corresponding to the kinetic energy of Auger electrons $E_{AES} = 412$ eV, (b) in the form of $Ti_{10}O_{19}$ ($E_{AES} = 415$ eV), and next (c) in the form of the intermetallic compounds NiTi ($E_{AES} = 418$ eV). An asymmetry of the Ti Auger (LMV) line was observed. The determined asymmetry equals $AR = I_g/I_d = 0.81$. This is caused by binding of titanium atoms with oxygen atoms and by titanium oxide formation. Analysis of the asymmetry of Ti by comparison with TiO and TiO_2 and assuming linearity of the asymmetry coefficient suggests that the Ti Auger line corresponds to the presence of nonstoichiometric Ti oxide, $TiO_{1.84}$, corresponding approximately to $Ti_{10}O_{19}$. The line asymmetry also indicates the presence of NiTi intermetallic alloy as a result of interactions between the composite layer and the matrix. This additional presence of a thin monomolecular layer of nonstoichiometric Ti oxide, $Ti_{10}O_{19}$, as well as intermetallic, NiTi, on the electrode surface probably affects the HER kinetics.

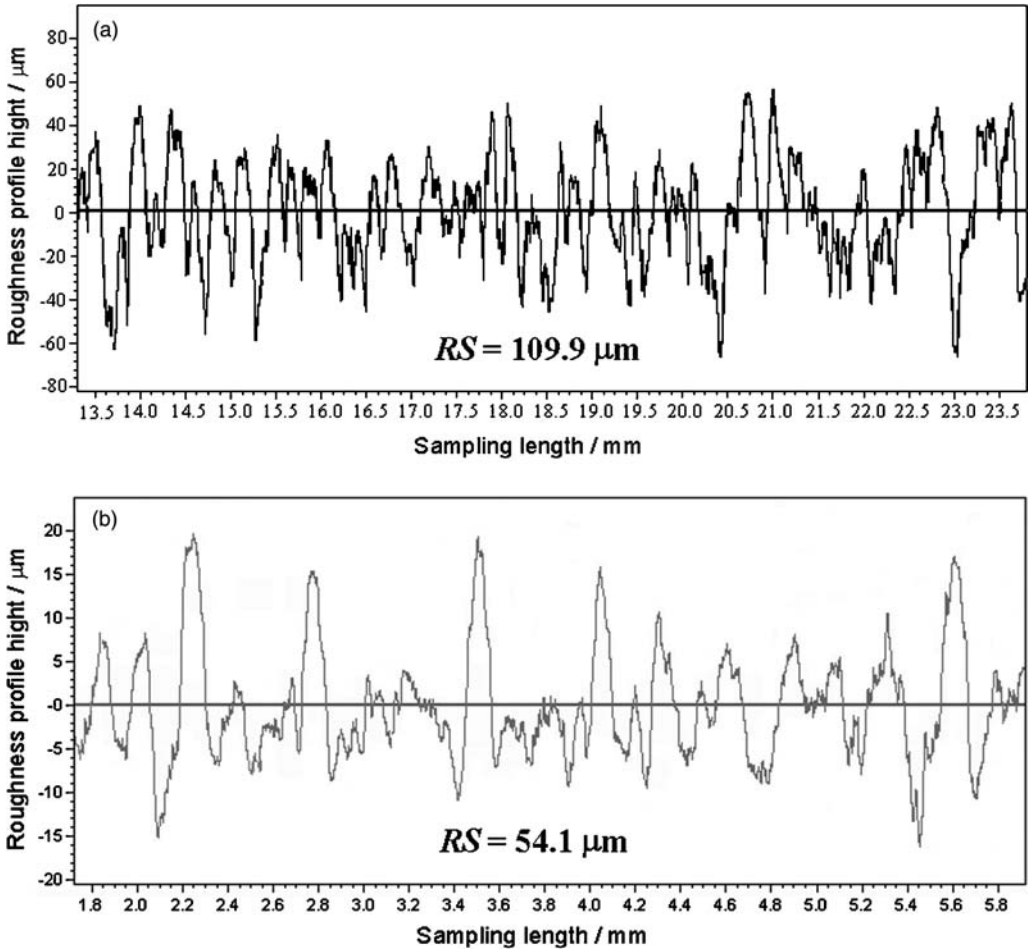

Fig. 2. Surface roughness profile of the Ni–P + TiO_2 + Ti layer before (a) and after heating at 400 °C (b).

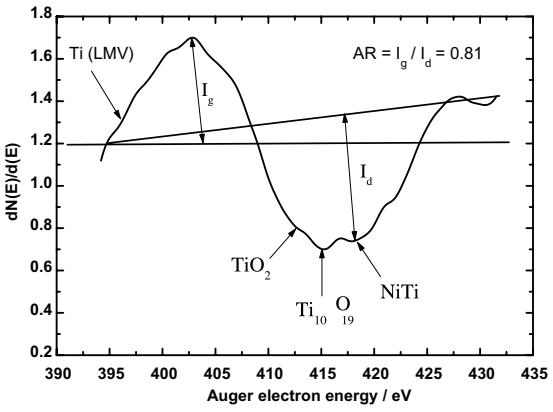

Fig. 3. Differential AES spectrum of Ti (LMV) for the surface of the Ni–P + TiO_2 + Ti layer.

3.3. *XRD measurements*

The XRD patterns for the Ni–P + TiO_2 + Ti layer (Figure 4(a)) show that the structure is composed of an amorphous matrix of Ni–P, on the basis of comparison of angles 2Θ with those obtained under the same conditions in previous work (Figure 1(a) and (b) of [8]). Additionally, the presence of crystalline TiO_2 and Ti phases was observed. This indicates embedding of Ti and TiO_2 powder into the Ni–P system during electrodeposition. Diffraction lines corresponding to nonstoichiometric Ti oxide phases were not observed, contrary to the observations found using the AES surface-sensitive method (Figure 3).

Table 1. Values of Auger line positions for the analysed elements [42]

Element	E_{AES}/eV
Ti	418
O	510
Ni	848

Markedly different XRD patterns were obtained for the layer heated at 400, 500 and 800 °C (Figure 4 (b)–(d)). The broad diffraction line corresponding to the Ni–P matrix (Figure 4(a)) disappeared and new ones, corresponding to the new phases of crystalline Ni and the nickel phosphide, Ni_5P_2, were formed. This means that heating those samples above 400 °C causes Ni–P matrix crystallization. Additionally, for the electrode heated at 800 °C, the diffraction lines corresponding to another new phase, $NiTiO_3$, the result of interaction between the nickel Ni matrix and Ti, is observed. All XRD results obtained for the heated layers revealed the presence of sharp lines arising from the diffraction by TiO_2 and Ti. Heating at 400, 500 and 800 °C caused

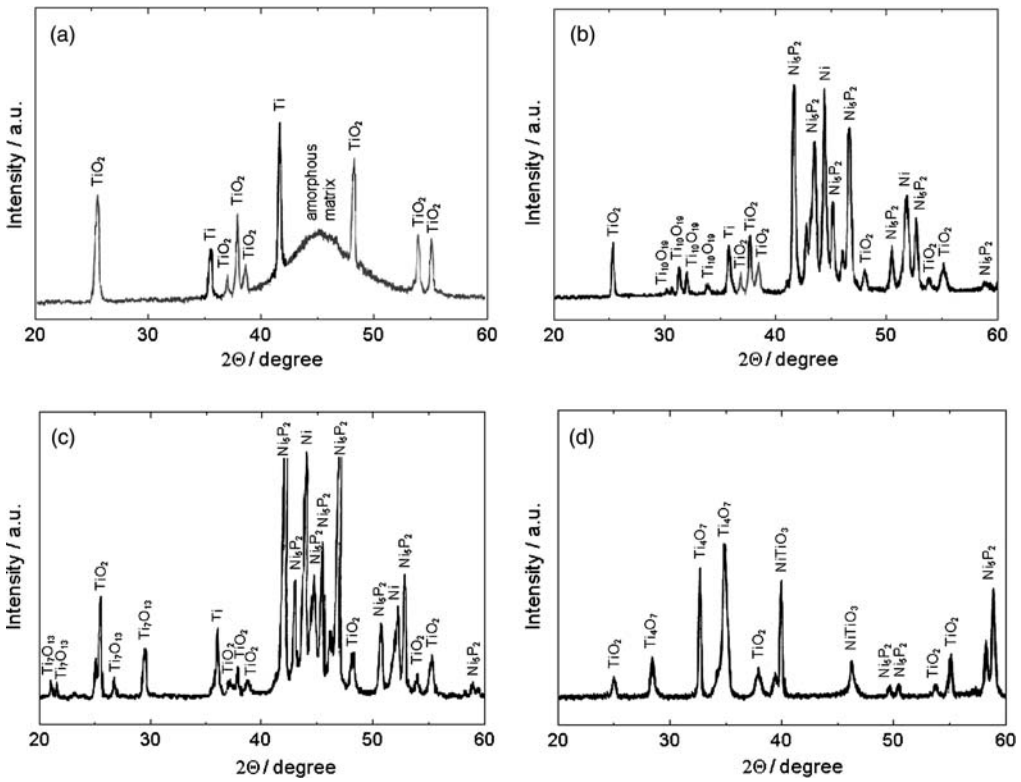

Fig. 4. XRD patterns of the Ni–P + TiO_2 + Ti layer before (a) and after heating at 400 °C (b), 500 °C (c), and at 800 °C (d).

formation of sharp lines corresponding to the new phases: $Ti_{10}O_{19}$, Ti_7O_{13} and Ti_4O_7, respectively. It should be added that all nonstoichiometric Ti oxides were formed as a consequence of partial TiO_2 reduction by Ti powder embedded in the layer. The results show that under the proposed heat treatment conditions it is possible to obtain new electrode materials containing nonstoichiometric Ti oxides. The electrochemical activity of the layers towards the HER may depend on the facility with which Ti oxides reduce/adsorb H.

3.4. *Steady-state polarization*

All Tafel curves obtained on Ni–P + TiO_2 + Ti layers, before (A) and after heat treatment at 400 (B), 500 (C) and 800 °C (D), were characterized by one slope in the whole potential range studied, Figure 5. The Tafel kinetic parameters (considering the geometric surface area), that is slope, b, exchange current density, j_0, and the overpotential at $j = 100$ mA cm^{-2}, η_{100}, are shown in Table 2. Kinetic parameters were obtained on two electrodes of each type. These results were reproducible.

All the layers are characterized by a high Tafel slope. Their physical stability and the adhesion to the substrate after three days of polarization with $j = 100$ mA cm^{-2} at 25 °C were very good. The layers obtained after heat treatment (B, C, D) are characterized by a lower Tafel slope. The lowest b value of -152 mV dec^{-1} was observed for electrode B.

The apparent values of j_0 determined on electrode A and heated layers B, C, D are comparable

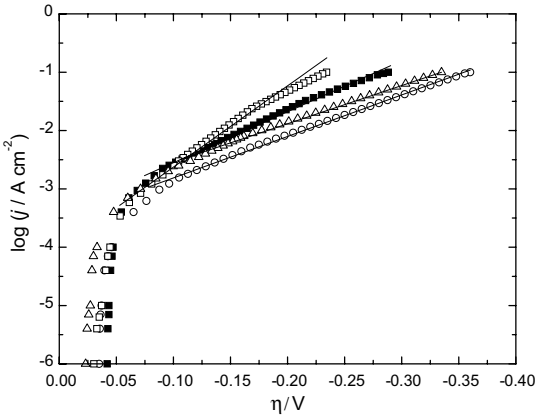

Fig. 5. Steady-state polarization curves for the HER in 5 M KOH at 25 °C on the Ni–P + TiO_2 + Ti electrode directly after deposition (○) and after heating in argon at 400 °C (□), at 500 °C (△), and at 800 °C (■). Continuous lines are linear approximations of the Tafel curves.

Table 2. Kinetic parameters obtained from the steady-state polarization curves for the HER in 5 M KOH at 25 °C on the Ni–P + TiO_2 + Ti layer before (A) and after heating in argon at 400 °C (B), at 500 °C (C), and at 800 °C (D)

Electrode	b /mV dec^{-1}	j_0 /A cm^{-2}	η_{100} /mV
Ni–P + TiO_2 + Ti (A)	−218	5.40×10^{-3}	−360
Ni–P + TiO_2 + $Ti_{10}O_{19}$ (B)	−152	1.38×10^{-3}	−288
Ni–P + TiO_2 + Ti_7O_{13} (C)	−188	1.35×10^{-3}	−334
Ni–P + TiO_2 + Ti_4O_7 (D)	−176	1.31×10^{-3}	−234

(10^{-3} A cm^{-2}). However, the highest value j_0 of 5.4 A cm^{-2} was observed for electrode A. This suggests the effect of composite layer surface development on the HER rate. On the other hand, the values of η_{100}, determined for the heated electrodes, range from −288 mV (electrode B) to −234 mV (electrode D), and are larger than the value of −360 mV obtained on electrode A (Table 2). This means that heating the Ni–P + TiO_2 + Ti layer under the proposed conditions leads to enhanced HER kinetics as compared to the starting material. Moreover, the deposit phase composition also influences the HER. The increase in electrochemical activity of Ni–P + TiO_x layers may be related to the presence of nonstoichiometric Ti oxides. Creation of new active centres on the electrode surface influences the activity more than the simple effect of surface area increase. Although the main purpose of this work was fundamental, the electrodes produced are attractive candidates as novel electrode materials in practical water electrolysis.

3.5. *Electrochemical impedance spectroscopy*

The EIS method was also used to study the electrolyte|electrode interfacial properties and kinetics of the HER. It has been reported [1–5,28–30] that on solid electrodes a.c. impedance plots deviate from the classical Randles' equivalent circuit. To explain the a.c. behaviour of the investigated electrodes, three other models were used [1,3–5,11–16,31–33].

In a simple CPE model [1,3–5,33] the double-layer capacitance, C_{dl}, is substituted by a constant phase element (CPE). Its impedance is [34]:

$$\widehat{Z}_{CPE} = \frac{1}{T(j\omega)^{\phi}} \tag{1}$$

where T is the capacitance parameter (in F cm^{-2} s$^{\phi-1}$), which may depend on the electrode potential, and $\phi \leqslant 1$ is a dimensionless parameter related to the constant phase angle, $\alpha = 90°(1 - \phi)$ [12]. The CPE is in parallel with the faradaic impedance, $\widehat{Z}_f$, usually represented as a simple charge-transfer resistance: $\widehat{Z}_f = R_{ct} = 1/A$ [30]. The average double-layer capacitance may be estimated as [34]

$$T = \overline{C}_{d1}^{\phi}(R_s^{-1} + A)^{1-\phi} \tag{2}$$

The CPE model explains the impedance behaviour of an electrode containing shallow pores [12]. It has four adjustable parameters: R_s, A, T and ϕ, and leads to a rotated semicircle on the Nyquist plot.

De Levie [35] proposed a porous electrode model in the absence of concentration polarization. This model describes the impedance of an electrode covered with deep cylindrical pores and its modified version, according to the Equations 3 and 4, was successfully applied earlier [12–16] for Raney Ni based materials:

$$\widehat{Z} = R_s + (R_{\Omega,p}/\Lambda^{1/2})\coth(\Lambda^{1/2}) \tag{3}$$

where

$$\Lambda = [1 + (j\omega)^{\phi}A_pB_p]/A_p \tag{4}$$

$A_p = aR_{ct}$, $B_p = T/a$, $a = r/2\rho l^2$, $R_{\Omega,p} = \rho l/n\pi r^2$, n is the number of pores per cm^2, r is the pore radius, l is the pore length, ρ is the solution specific resistance. The porous electrode model predicts the formation of a straight line at 45° at high frequencies followed by a semicircle at lower frequencies on the Nyquist plot and has five adjustable parameters: R_s, A_p, B_p, ϕ and $R_{\Omega,p}$.

The third, two-CPE model, consists of the solution resistance in series with two parallel CPE-R elements. This model explains the impedance behaviour of an electrode containing pear-shape pores [1,3,4,12–16]. This equivalent circuit produces two semicircles on the Nyquist plot where the high-frequency semicircle is related to the surface porosity, similarly to a high-frequency straight line observed for cylindrical pores, and the low-frequency semicircle is related to the charge-transfer process. That model has seven parameters: R_s, A_1, A, T_1, ϕ_1, T and ϕ.

EIS measurements were performed on Ni–P + TiO_2 + Ti electrodes before (A) and after heat treatment (B, C, D) in the potential range in which the steady-state polarization curves were recorded. All electrodes displayed two semicircles on the complex-plane plots, but the diameter of the first one was independent of overpotential, while the second one varied with overpotential and was attributed to the HER. This behaviour is similar to that observed for porous electrodes covered with pear-shaped pores [12]. In this case the first semicircle was attributed to the porosity of the electrode and the second to the kinetics of the HER. Typical impedance curves obtained on electrode A are shown in Figure 6(a)–(d).

The impedance plots were analysed using the modified CNLS program. The best fit to the experimental data for A, B, C and D electrodes was obtained using the two-CPE model. The approximations of the Nyquist plots (Figure 6) are very good. The Bode phase-angle plots, displayed in Figure 7, also confirm good quality approximations. Figure 8 presents an example of the CNLS approximation of impedances obtained in 5 M KOH at $\eta = -278$ mV at 25 °C on electrode A. The high-frequency part of the plot (Figure 8(a)), differs systematically from the approximations by the CPE and porous models. Therefore, in further approximations the two-CPE model was used.

The diameter of the first semicircle did not change with overpotential. The experimental impedance curves were fitted to the two-CPE model with the A_1, T_1 and ϕ_1 for the first high frequency flat part of the impedance diagram and $A = 1/R_{ct}$, T and ϕ for the low frequency part, connected with the faradaic process. The results

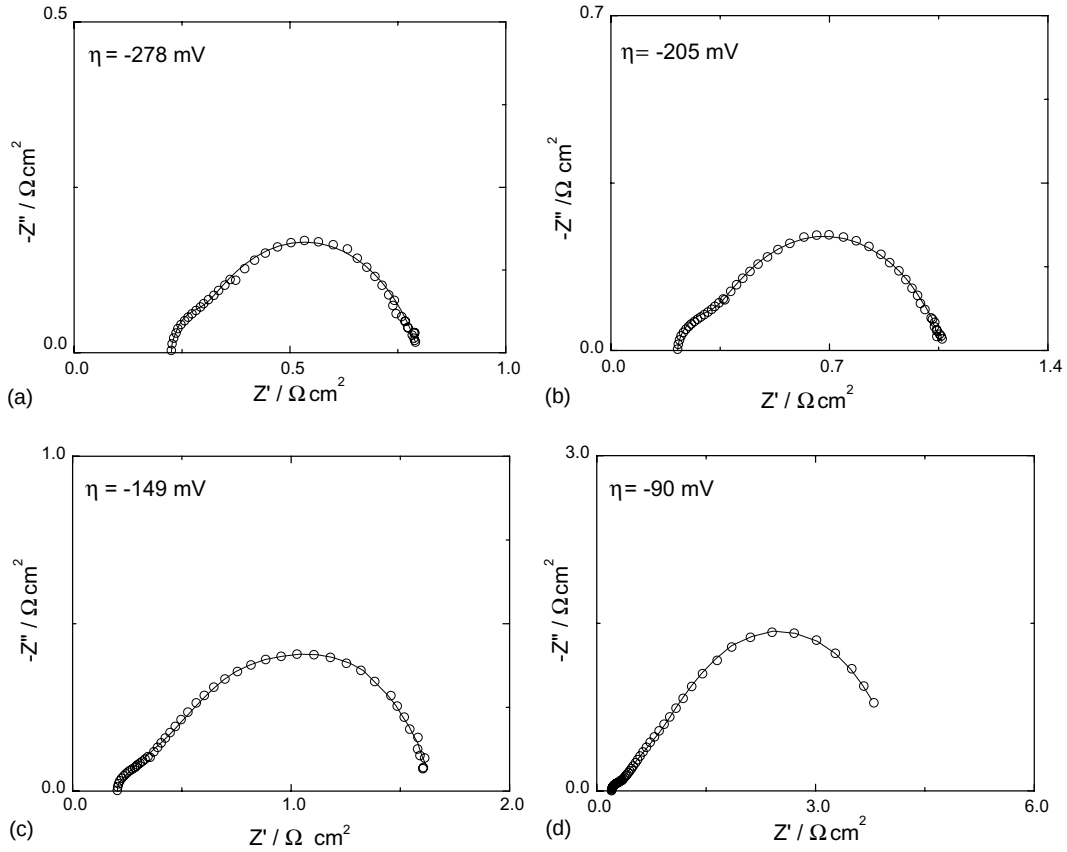

Fig. 6. Complex-plane plots obtained on the Ni–P + TiO_2 + Ti electrode in 5 M KOH at 25 °C at various overpotentials (a–d). Symbols (○) are experimental data; continuous lines indicate fitted data using CNLS method and two-CPE model.

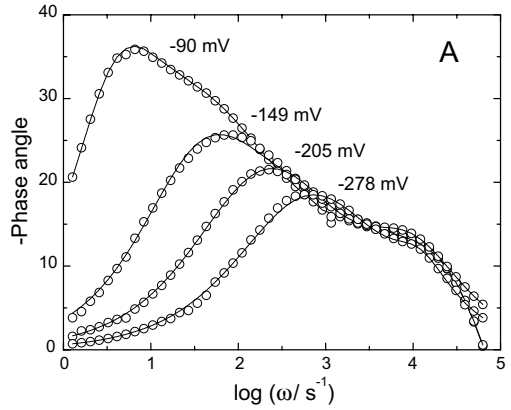

Fig. 7. Phase-angle Bode plots obtained for the HER in 5 M KOH at 25 °C on the Ni–P + TiO_2 + Ti electrode (A). Points (○) are experimental data, continuous lines are CNLS approximation.

are shown in Table 3. Figure 9 presents the double-layer capacitance (a) and the parameter ϕ (b) as functions of overpotential. The double-layer capacitance was estimated using Equation 2 [34]. The values of C_{dl} are generally independent of overpotential. For the Ni–P + TiO_2 + Ti electrode the average C_{dl} value is 2 mF cm^{-2}. The average C_{dl} value of the electrode heated at 400 °C is the largest and equals 5 mF cm^{-2}, higher than those obtained for electrodes heated at 500 °C ($C_{dl} = 1.6$ mF cm^{-2}) and 800 °C ($C_{dl} =$ 0.47 mF cm^{-2}), indicating that the heat treatment of the Ni–P + TiO_2 + Ti layer above 400 °C causes a decrease in C_{dl}. Small variations of C_{dl} with overpotential may indicate changes in the electrochemical behaviour of Ti oxides. The presence of both TiO_2 and nonstoichiometric Ti oxides may cause synergetic effects for the HER.

The values of the parameter ϕ for the Ni–P + TiO_2 + Ti electrode before and after heating at 500 °C are close to 1, and for the electrodes heated at 400 and 800 °C the value of ϕ decreases to about 0.75 (at higher overpotentials). It has been suggested that deviation of the parameter ϕ from 1 is associated with surface roughness. However, it has been reported that this phenomenon might also be connected with surface heterogeneity and ionic adsorption [12, 36, 37].

The dependence of the logarithm of the inverse charge-transfer resistance A against η is shown in Figure 10. These dependences are linear for all electrodes with slope equal to the Tafel slopes (Table 2). All the logarithmic slopes are a little larger than the value of −120 mV dec^{-1} predicted for the Volmer–Heyrovský mechanism. This is likely due to the distributed kinetics on composite materials. Surface heterogeneity causes a distribution of hydrogen adsorption energies on different parts of the electrode. Nevertheless, the slopes may be successfully explained by the Volmer–Heyrovský reaction mechanism.

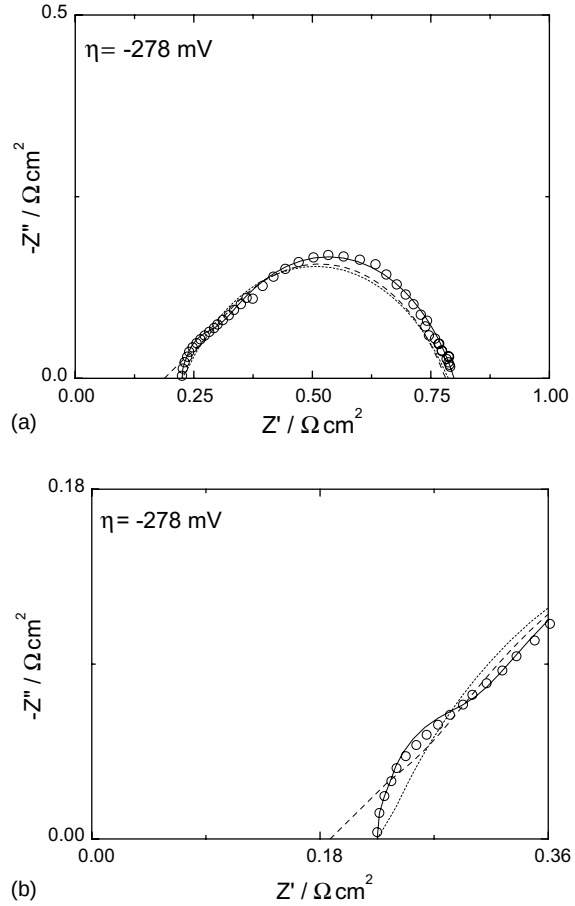

Fig. 8. Complex-plane plots obtained on the Ni–P + TiO_2 + Ti electrode at $\eta = -278$ mV, in 5 M KOH, at 25 °C, fitted to different models: continuous line (—) for two-CPE model, dot line (···) for porous model, and dash dot line (- - -) for one-CPE model; (b) in the whole range of frequencies and (a) in high frequency range.

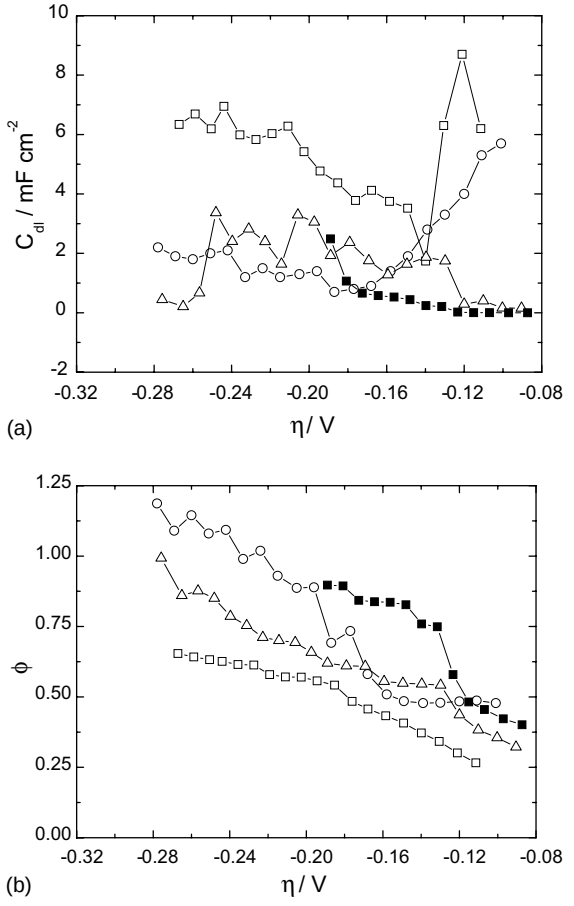

Fig. 9. Dependence of (a) double-layer capacitance, C_{dl}, and (b) ϕ parameter on overpotential for the HER in 5 M KOH at 25 °C on the Ni–P + TiO_2 + Ti electrode: directly after deposition (○) and after heating in argon at 400 °C (□), at 500 °C (△), and at 800 °C (■).

The kinetic parameters of the HER were obtained by simultaneous fitting of the steady-state polarization curves and the charge-transfer resistances from the EIS to the corresponding kinetic equations using the NLS method. A very good approximation was observed (Figures 5 and 10). The kinetic parameters, together with their standard deviations, are displayed in Table 3. It was sufficient to assume the Volmer–Heyrovský mechanism to explain the experimental data. Because the determination was carried out at sufficiently negative overpotentials in the Tafel range only an average rate constant, $\bar{k}_{av}$, could be determined:

$$\bar{k}_{av} = \frac{1}{(1/k_1) + (1/k_2)} \qquad (5)$$

It was possible to fit the Tafel plots and the EIS data together for all investigated electrodes.

The intrinsic activity of the electrodes may be evaluated from the apparent experimental values of the exchange current densities, j_0, and the values of kinetic parameters, $\bar{k}_{av}$, divided by the roughness factor, R_f [1, 3–5, 11–16]. The roughness factor was estimated from the ratio of the average double-layer capacitance of the tested electrode, C_{dl}, and the double-layer capacitance of a smooth metallic electrode, $R_f = C_{dl}/20\ \mu F\ cm^{-2}$ [11]. The apparent and the real (per unit of a real surface area) results are presented in Table 3.

The highest intrinsic activity for the HER was observed on electrode B. The intrinsic activity, $\bar{k}_{av}/R_f$, of that electrode is one order of magnitude larger than

Table 3. Comparison of the apparent and the real kinetic parameters of the HER obtained from steady-state and a.c. impedance experiments in 5 M KOH on the Ni–P + TiO_2 + Ti electrode before and after heat treatment

Electrode	$\bar{k}_{av}$ /mol cm^{-2} s^{-1}	α	R_f	j_0/R_f /A cm^{-2}	$k_{intrinsic} = \bar{k}_{av}/R_f$ /mol cm^{-2} s^{-1}
Ni–P + TiO_2 + Ti (A)	$(6.09 \pm 0.04) \times 10^{-9}$	0.35 ± 0.01	101	5.34×10^{-5}	6.02×10^{-11}
Ni–P + TiO_2 + $Ti_{10}O_{19}$ (B)	$(1.98 \pm 0.14) \times 10^{-8}$	0.29 ± 0.04	65	5.45×10^{-5}	3.04×10^{-10}
Ni–P + TiO_2 + Ti_7O_{13} (C)	$(5.69 \pm 0.05) \times 10^{-9}$	0.26 ± 0.01	80	1.68×10^{-5}	7.11×10^{-11}
Ni–P + TiO_2 + Ti_4O_7 (D)	$(3.88 \pm 0.05) \times 10^{-9}$	0.21 ± 0.01	24	2.12×10^{-5}	1.61×10^{-10}

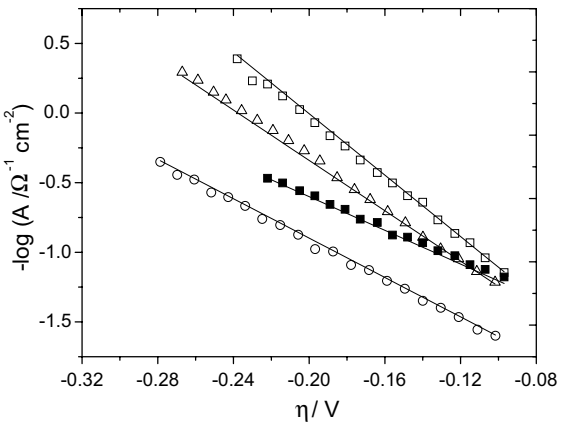

Fig. 10. Dependence of charge-transfer resistance inverse, $A = 1/R_{ct}$, on overpotential for the HER in 5 M KOH at 25 °C; symbols as in Figure 9.

that of electrode A. Comparison of the electrode materials, Table 3, $\bar{k}_{av}$, indicates that the apparent activity of B is one order of magnitude larger than that of the Ni–P + TiO_2 + Ti electrode. One order of magnitude of the apparent rate constant increase originates mainly from the increase in the intrinsic activity, $k_{real}(B)/k_{real}(A) \cong 5.1$ (Table 3). Such comparison of the apparent and real parameters in Table 3 reveals that the increase in activity of the electrode heated at 400 °C is achieved mainly by the increase in intrinsic activity.

It seems that the synergetic effect, which is responsible for that electrode activity, arises from the presence of $Ti_{10}O_{19}$ as well as the intermetallic NiTi. Therefore, the Volmer–Heyrovský mechanism of the HER on those electrodes should include the participation of nonstoichiometric Ti oxides, and may be similar to that reported elsewhere [8]. It can be described by the following equations:

$$Ti_{10}O_{19} + H_2O + e^- \rightarrow Ti_{10}O_{19}H + OH^- \text{ Volmer step} \quad (6)$$

$$Ti_{10}O_{19}H + H_2O + e^- \rightarrow Ti_{10}O_{19} + H_2\uparrow + OH^- \text{ Heyrovský step} \quad (7)$$

Participation of nonstoichiometric Ti oxides in the HER arises from the ability of the hydrogen atoms to attach to the free oxygen electron pairs. It may be also assumed that the NiTi intermetallic compound is a phase having an ability to accumulate hydrogen in its crystal lattice. Certainly, the presence of NiTi affects the potential nonhomogeneity on the electrode surface and thus influences the HER.

4. Conclusions

Composite Ni–P + TiO_2 + Ti layers can be prepared by electrodeposition from a nickel-plating bath containing suspensions of TiO_2 and Ti powders. The layers exhibit an amorphous nickel matrix in which the crystalline TiO_2 and Ti components are embedded. On such a surface, the nonstoichiometric Ti oxide, $Ti_{10}O_{19}$, and intermetallic compounds, NiTi, formed during the electrodeposition at the boundary of the TiO_2 and Ti grains, and the Ni–P matrix, are additionally present. The heat treatment of such layers in argon leads to Ni–P matrix crystallization and nonstoichiometric Ti oxide formation: these are visible on the X-ray patterns.

It was established that the HER, on all the investigated electrodes, proceeds via the Volmer–Heyrovský reaction mechanism. An increase in activity towards the HER, which occurs after heating the electrodes, is associated with TiO_2 reduction and the formation of nonstoichiometric Ti oxides: $Ti_{10}O_{19}$ (400 °C), Ti_7O_{13} (500 °C) and Ti_4O_7 (800 °C) which influence that process. The best electrode for the HER in 5 M KOH at 25 °C is Ni–P + TiO_2 + $Ti_{10}O_{19}$ (electrode B). It has been postulated that the increase in activity of heated electrodes is due to the presence of nonstoichiometric Ti oxides and NiTi intermetallics, as compared with the as-deposited electrode. The properties of the Ti oxides and their facility for H reduction/adsorption influence the HER kinetics on heated electrodes.

Acknowledgements

Financial support from the Polish Committee for Scientific Research (Project 7 T08A 046 19) is gratefully acknowledged. The authors warmly thank Professor J. Cybo and Dr G. Służatłek for their assistance with the Form Talysurf surface analyser.

References

1. A. Lasia, *in* B.E. Conway and R.E. White (Eds), 'Modern Aspects of Electrochemistry', Vol. 35 (Kluwer Academic/Plenum Publishers, New York, 2002), p. 1.
2. A. Lasia, *in* B.E. Conway, J. Bockris and R.E. White (Eds), 'Modern Aspects of Electrochemistry', Vol. 32 (Kluwer Academic/Plenum Publishers, New York, 1999), p. 143.
3. J. Panek, A. Serek, A. Budniok, E. Rówiński and E. Łągiewka, *Int. J. Hydrogen Energy* **28** (2003) 169.
4. B. Łosiewicz, A. Budniok, E. Rówiński, E. Łągiewka and A. Lasia, *Int. J. Hydrogen Energy* **29** (2004) 145.
5. A. Lasia, *in* W. Vielstich, A. Lamm and H.A. Gasteiger (Eds), 'Handbook of Fuel Cells. Fundamentals, Technology and Applications', Vol. 2, Part 4 (John Wiley & Sons, Chichester, UK, 2003), pp. 416–440.
6. R. Rausch and H. Wendt, *J. Electrochem. Soc.* **9** (1996) 143.
7. A. Gruszka and A. Budniok, *Adv. Perform. Mater.* **6** (1999) 141.
8. D. Gierlotka, E. Rówiński, A. Budniok and E. Łągiewka, *J. Appl. Electrochem.* **27** (1997) 1.
9. B. Łosiewicz, A. Stępień, D. Gierlotka and A. Budniok, *Thin Sol. Films* **349** (1999) 43.
10. I. Napłoszek-Bilnik and A. Budniok, *Composites* **2** (2002) 63.
11. R. Karimi Shervedani and A. Lasia, *J. Electrochem. Soc.* **144** (1997) 511.
12. R. Karimi Shervedani and A. Lasia, *J. Electrochem. Soc.* **144** (1997) 8.

13. R. Karimi Shervedani and A. Lasia, *J. Appl. Electrochem.* **29** (1999) 979.
14. R. Karimi Shervedani and A. Lasia, *J. Electrochem. Soc.* **145** (1998) 2219.
15. L. Chen and A. Lasia, *J. Electrochem. Soc.* **140** (1993) 2464.
16. C. Hitz and A. Lasia, *J. Electroanal. Chem.* **500** (2001) 213; C. Hitz and A. Lasia, *J. Electroanal. Chem.* **532** (2002) 133.
17. P.A. Gay, P. Berçot and J. Pagetti, *Surf. Coat. Technol.* **140** (2001) 147.
18. S. Takeda, S. Suzuki, H. Odaka and H. Hosono, *Thin Sol. Films* **392** (2001) 338.
19. S. Survilienë, L. Orlovskaja, G. Bikulcius and S. Biallozor, *Surf. Coat. Technol.* **137** (2001) 230.
20. S. Rodrigues, N. Munichandraiah and A.K. Shukla, *Bull. Mater. Sci.* **23** (2000) 383.
21. E.B. Castro, M.J. de Giz, E.R. Gonzalez and J.R. Vilche, *Electrochim. Acta* **42** (1997) 951.
22. A. Takasaki, Y. Furuya, K. Ojima and Y. Taneda, *J. Alloy Compd.* **224** (1995) 269.
23. T. Mizuno and M. Enyo, *Denki Kagaku* **63** (1995) 719.
24. J.R. Macdonald, J. Schoonman and A.P. Lehner, *J. Electroanal. Chem.* **131** (1982) 77.
25. P.W. Palmberg, G.E. Riach, R.E. Weber and N.C. MacDonald, 'Handbook of Auger Electron Spectroscopy' (Physical Electronics Industries, Edina, Minessota, 1976).
26. E. Rówiński and E. Łągiewka, *Arch. Mater. Sci.* **20** (1999) 241.
27. E. Rówiński, *Surf. Sci.* **411** (1998) 316.
28. J.O'M. Bockris, J. McBree and L. Nanis, *J. Electrochem. Soc.* **112** (1965) 1025.
29. D.A. Harrington and B.E. Conway, *J. Electroanal. Chem.* **221** (1987) 1.
30. D.A. Harrington and B.E. Conway, *Electrochim. Acta* **32** (1987) 1703.
31. A. Lasia and A. Rami, *J. Electroanal. Chem.* **294** (1990) 123.
32. P. Los, A. Lasia and H. Ménard, *J. Electroanal. Chem.* **360** (1993) 101.
33. A. Lasia, *Curr. Topics Electrochem.* **2** (1993) 239.
34. G.J. Brug, A.L.G. van den Eeden, M. Sluyters-Rehabach and J.H. Sluyters, *J. Electroanal. Chem.* **176** (1984) 275.
35. R. de Levie, *in* P. Delahay (Ed), 'Adv. Electrochem. Electrochem. Eng.' Vol. 6 (Interscience, New York, 1967), p. 326.
36. H. Dumont, P. Los, L. Brossard, A. Lasia and H. Ménard, *J. Electrochem. Soc.* **139** (1992) 2143.
37. T. Pajkossy, *J. Electroanal. Chem.* **364** (1994) 11.